Charge-Controlled Nanoprecipitation as a Modular Approach to Ultrasmall Polymer Nanocarriers: Making Bright and Stable Nanoparticles

Andreas Reisch,* Anne Runser, Youri Arntz, Yves Mély, and Andrey S. Klymchenko*

Laboratoire de Biophotonique et Pharmacologie, UMR 7213 CNRS, Université de Strasbourg, Faculté de Pharmacie, 74 Route du Rhin, 67401 Illkirch, France

ABSTRACT Ultrasmall polymer nanoparticles are rapidly gaining importance as nanocarriers for drugs and contrast agents. Here, a straightforward modular approach to efficiently loaded and stable sub-20-nm polymer particles is developed. In order to obtain ultrasmall polymer nanoparticles, we investigated the influence of one to two charged groups per polymer chain on the size of particles obtained by nanoprecipitation. Negatively charged carboxylate and sulfonate or positively charged trimethylammonium groups were introduced into the polymers poly(D,L-lactide-*co*-glycolide) (PLGA), polycaprolactone (PCL), and poly(methyl methacrylate) (PMMA). According to dynamic light scattering, atomic force and electron microscopy, the presence of one to two charged groups per polymer chain can strongly reduce the size of polymer nanoparticles made by nanoprecipitation. The particle size can be further decreased to less than 15 nm by decreasing the concentration of polymer in the solvent used for nanoprecipitation. We then show that even very small nanocarriers of 15 nm size preserve the capacity to encapsulate large amounts of ionic dyes with bulky counterions at efficiencies >90%, which generates polymer nanoparticles 10-fold brighter than quantum dots of the same size. Postmodification of their surface with the PEG containing amphiphiles Tween 80 and pluronic F-127 led to particles that were stable under physiological conditions and in the presence of 10% fetal bovine serum. This modular route could become a general method for the preparation of ultrasmall polymer nanoparticles as nanocarriers of contrast agents and drugs.

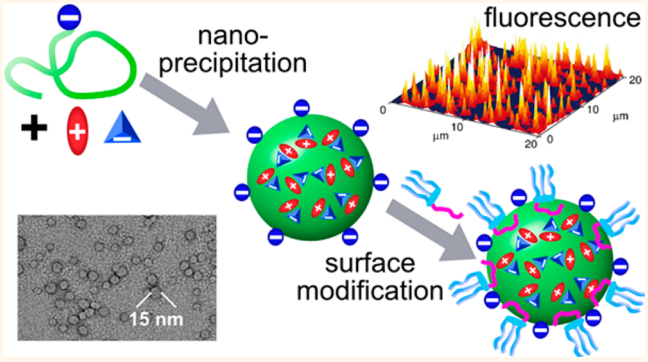

KEYWORDS: polymer nanoparticles · nanocarriers · size · nanoprecipitation · encapsulation efficiency · fluorescent nanoparticles · surface modification

In the past decades, polymer nanoparticles (polymer NPs) have gained a high degree of importance as carriers in drug delivery.[1−3] They allow facile encapsulation of a vast choice of small molecules and their controlled release over time and/or following external stimuli. However, this research was mainly focused on NPs in the range of 50 to 250 nm, because they should be small enough to avoid fast clearance by the reticuloendothelial system,[4] but large enough to avoid rapid elimination through the kidneys.[5] Though the field of NPs below 50 nm is underexplored, recent works showed that these NPs may have a great future in biomedical research. First, the enhanced permeation and retention effect (EPR) that allows passive targeting of tumors is further enhanced for NPs of 50 nm and less.[6−8] Second, some NPs of very small size can enter cells by crossing directly the membrane barrier,[9,10] unlike larger particles, which enter the cells by endocytosis or pinocytosis.[11] Finally, polymeric nanocarriers are rapidly gaining interest as contrast agents and especially as ultrabright fluorescent markers,[12−15] a field, up to now, dominated by inorganic particles especially by quantum dots (QDs).[16,17] For fluorescence imaging, NPs should be as small as possible, in order to be useful for detecting/tracking biomolecules[18,19] and super-resolution microscopy,[15,20] while being able to access small intracellular compartments.[21] These

* Address correspondence to andreas.reisch@unistra.fr, andrey.klymchenko@unistra.fr.

Received for review January 12, 2015 and accepted April 20, 2015.

Published online April 20, 2015
10.1021/acsnano.5b00214

applications require robust and flexible synthesis of nanocarriers, combining ultrasmall size, efficient loading, adjustable core and surface properties.[18,22] The latter have notably to be adapted to the use in biological environments, which impose challenges in view of particle stabilization and suppression of nonspecific interactions.[23,24]

The classical techniques used for the preparation of NPs below 50 nm are based on *in situ* polymerization (notably miniemulsion and microemulsion polymerization)[25,26] or on the formation of polymeric micelles from block copolymers.[27−30] Polymerization approaches have several limitations: (1) the molecules have to be stable in the conditions of polymerization; (2) the quantity of remaining monomers is difficult to control; and (3) relatively large concentrations of surfactant are needed, which complicates the control of the NP surface chemistry. In contrast, polymeric micelles can be directly assembled from block copolymers containing polyethylene glycol (PEG) as the hydrophilic part that forms a biocompatible shell preventing aggregation and nonspecific interactions.[31] However, achieving ultrasmall polymeric micelles requires generally short block copolymers with a high ratio of the hydrophilic to the hydrophobic block length.[32,33] This leads to a thick shell with respect to the core and a higher solubility of the individual block copolymers in water, thus decreasing the encapsulation efficiency and the stability of the resulting NPs, as well as increasing unwanted fast initial (burst) release of the encapsulated compounds.[34−39]

An alternative and straightforward approach for producing loaded polymer NPs is nanoprecipitation, also called solvent displacement. Nanoprecipitation only requires dissolving the polymer together with the small molecule cargo in a water miscible solvent, and adding this solution into a nonsolvent for the polymer, most often water.[40,41] Diffusion of the solvent into the aqueous phase (and of the water into the organic phase) leads to supersaturation and thus to the formation of polymer NPs encapsulating the cargo molecules. This simple and flexible protocol makes nanoprecipitation an attractive technique for producing loaded polymer NPs.[22,42−45] However, most particles formed by this technique have sizes in the range of 50 to 500 nm.[25,41,46−50] Recently, we described the synthesis of 40 nm NPs from poly(D,L-lactide-*co*-glycolide) (PLGA) by optimizing the mixing protocol and decreasing the polymer concentration.[15] This protocol enabled preparation of fluorescent polymer NPs several times brighter than QDs. We hypothesized that the charge at the end of the polymer chain might help in reducing the particle size. This is in line with scattered data in the literature, where the smallest particles are often obtained using polymers bearing charged groups or using charged surfactants.[41,46,51−53] However, no systematic study on the influence of polymer charge is available, and polymer charge has not been exploited to prepare ultrasmall polymer NPs.

In the present work we propose a modular approach for preparation of ultrasmall NPs with efficient dye loading based on charge-controlled nanoprecipitation and further stabilization of the NPs by surfactants. We first showed that nanoprecipitation into ultrasmall NPs can be controlled by one to two charged groups in a polymer. The concept was validated on polymers frequently used in the biomaterials field, namely poly(D,L-lactide-*co*-glycolide) (PLGA) and polycaprolactone (PCL), two biodegradable polyesters, and poly(methyl methacrylate) (PMMA), a nonbiodegradable, acrylic polymer. Optimizing the experimental conditions enabled preparation of particles of ~15 nm mean diameter. Despite their small size, the particles encapsulated almost quantitatively large amounts of dyes, leading to NPs more than 10 times as bright as QDs. Finally, the NP stability in biological media (salts and serum proteins) was ensured using PEGylated amphiphiles that formed very thin protective shells at the particle surface. Thus, our simple two-step modular approach enables preparation of ultrasmall polymer NPs stable in biological media and featuring excellent fluorescence brightness due to efficient encapsulation of organic dyes.

RESULTS

Modification of Polymers with Different Charged Groups. In order to investigate the influence of the charge of the polymer end groups, we modified the chain ends of PLGA and PCL (Figure 1). The PLGA used had one terminal carboxylic acid group, which allowed us introducing end groups through amide coupling using HBTU and HOBt with the corresponding amines: (1) amine terminated PEGs, to introduce neutral PEG with different chain lengths; (2) (2-aminoethyl)trimethylammonium chloride, to introduce positively charged trimethylammonium groups; and (3) taurine, to introduce negatively charged sulfonate groups. In order to evaluate the degree of modification of the end groups we employed NMR spectroscopy (Figure 2, Supporting Information Figure S1 for PCL and PMMA). For instance, the introduction of a PEG comprising 24 ethylene glycol (CH_2CH_2O) units led to the appearance of signals at 3.66, 3.64, 3.48, and 3.38 ppm corresponding to the CH_2 groups of the PEG. Together the intensity of these signals was 0.44 compared to one proton in one of the repeat units. The expected value for the total of 48 CH_2 groups of a PEG of 24 units at the end of a chain containing 185 lactic and 185 glycolic acid units would be $1/185 \times 2 \times 48 = 0.52$. This yields a degree of modification of the terminal acid groups of the PLGA of 85%. Taking into account that the reprecipitation procedure probably led to an increase of the mean molecular weight of the polymer, the actual degree of modification might even be higher than 85%. Similar

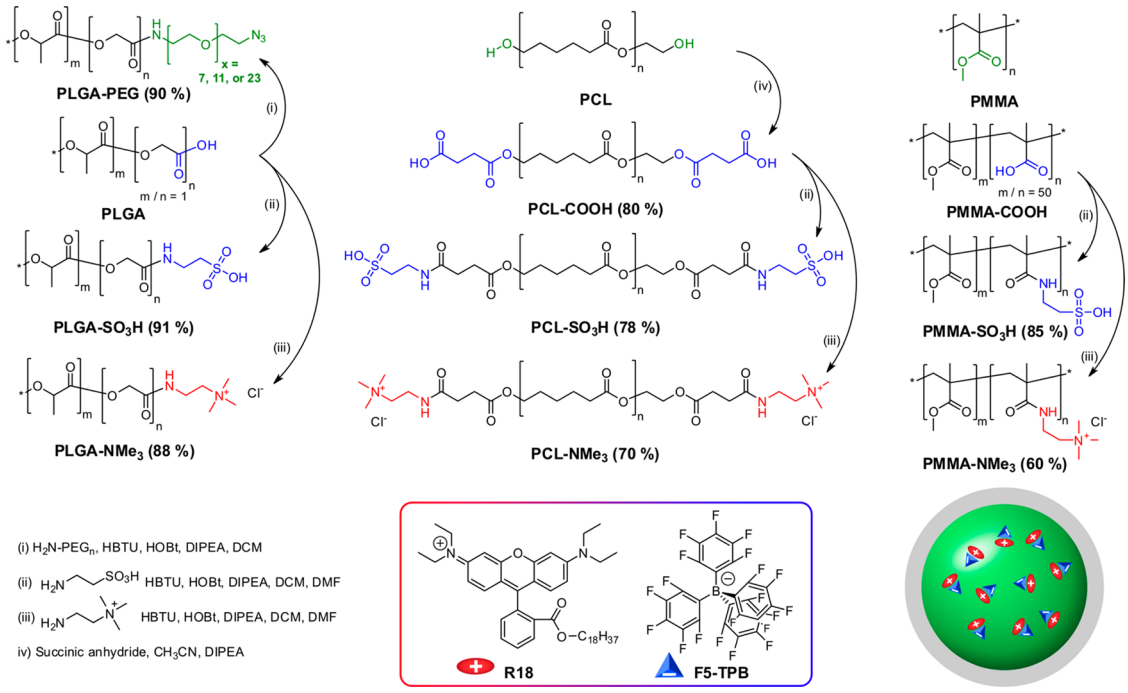

Figure 1. Chemically modified polymers used in this study and schematic view of synthesis of dye loaded NPs. Poly(D,L-lactide-*co*-glycolide) (PLGA) bearing a carboxylate group at one chain end, polycaprolactone (PCL) bearing hydroxyl groups at both chain ends, and a copolymer of poly(methyl methacrylate) (PMMA) with methacrylic acid were modified with PEG, carboxylate, sulfonate, and trimethylammonium groups. A salt of rhodamine B octadecyl ester (R18) with tetrakis-(pentafluorophenyl)borate (F5-TPB) as counterion was used as dye for encapsulation.

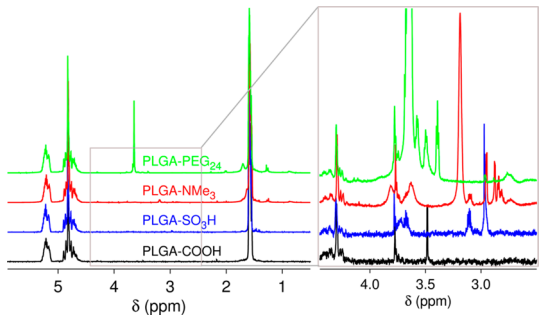

Figure 2. ^{1}H NMR spectra of parent PLGA (PLGA-COOH) and PLGA modified with different terminal groups.

analysis was applied to the other types of modification, yielding a degree of modification of 88 and 90% for trimethylammonium and sulfonate groups, respectively. The PCL used bears two terminal hydroxy groups, which were reacted with succinic anhydride to introduce carboxyl functionalities. The resulting spectra showed a multiplet at 2.63 ppm attributed to the CH_2 groups of the succinic amide (Supporting Information Figure S1). The associated intensity gave a degree of modification of around 80%. The resulting PCL-COOH was then reacted with taurine and 2-(aminoethyl)trimethylammonium chloride in the same way as PLGA, giving degrees of modification of 77 and 70% for introduction of the sulfonate and trimethylammonium groups, respectively, which accounts for the modification of both chain ends (*i.e.*, about 1.5 groups per chain). As a carboxylate bearing form of PMMA we used a copolymer of methyl methacrylate with 1.3% methacrylic acid (Figure 1), which corresponds on average to 2 carboxylate groups per chain. Reaction with taurine and 2-(aminoethyl) trimethylammonium chloride yielded a degree of modification of about 85 and 60%, respectively.

Influence of the End Groups on Particle Size and Zeta-Potential. The influence of a single polar group at the polymer chain end on the size of NPs, made by nanoprecipitation, was then investigated. Earlier we showed that nanoprecipitation of PLGA-COOH from acetonitrile solution into 20 mM phosphate buffer gave ~40 nm particles. To maximize the effect of charge we first performed nanoprecipitation of PLGA polymers bearing different end groups in Milli-Q water. Dynamic light scattering (DLS) showed that the size of the obtained NPs decreased in the following order with respect to the end groups PEG_{12} > PEG_{24} > COOH > NMe_3 > SO_3H (Figure 3a), for PLGA polymers of two different molecular weights (7000 and 24 000) (Figure 3). The size decreased from 150 nm for PEG_{12} end groups to 25 nm for SO_3H end groups. Noticeably, NPs obtained from PLGA-COOH, *i.e.*, the parent PLGA, were the largest among polymers bearing charged groups. Transmission electron microscopy (TEM) confirmed the observed trends in the particle sizes (Figure 3c), but gave somewhat smaller mean size values as compared to DLS data. Though the polydispersity index given by DLS remained below 0.2 for all particles, TEM showed some inhomogeneities in the

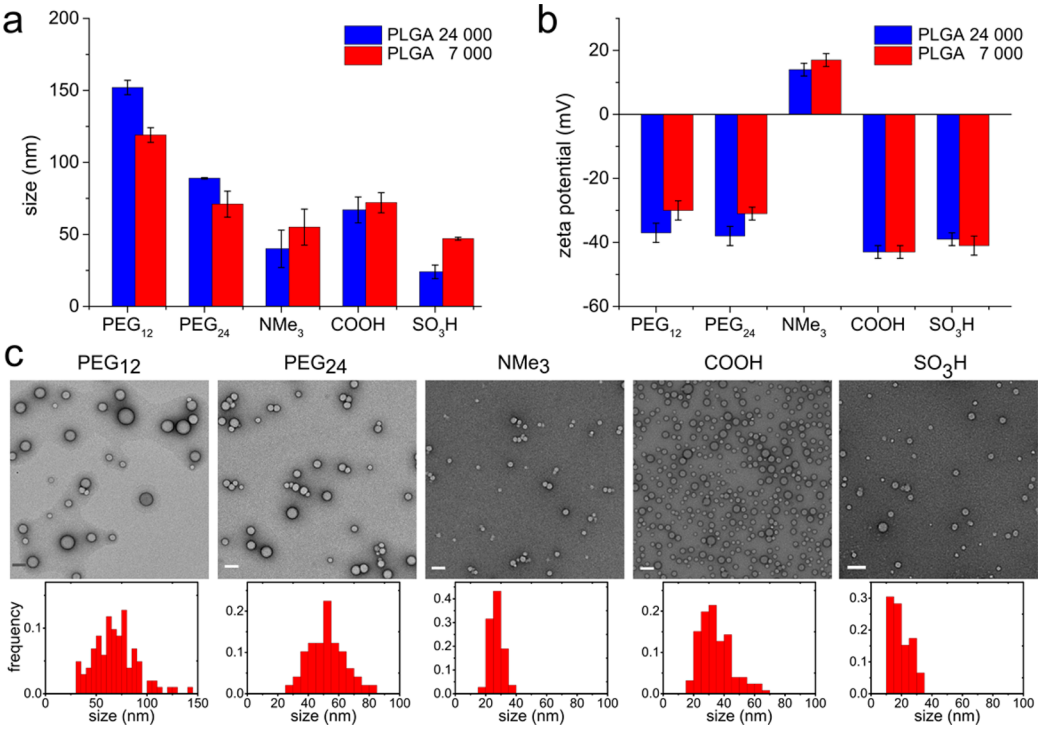

Figure 3. Influence of the end groups on size and zeta potential of PLGA nanoparticles. (a) Size and (b) zeta potential of nanoparticles made from PLGA with different end groups as measured by dynamic light scattering. Nanoparticles were made from PLGA of two different molecular weights (24 000 and 7000). (c) TEM images and size histograms of nanoparticles from PLGA 24 000 with different end groups. In all cases the PLGA concentration was 2 mg mL^{-1} in acetonitrile, and water was used as the nonsolvent. Values for the size are averages of volume distribution mean values; the error bars correspond to s.e.m. The scale bars correspond to 100 nm.

particle sizes for the PEGylated PLGA. The zeta potentials of the obtained NPs were clearly negative for PLGAs with carboxy and sulfonate end groups (−40 mV) and positive for PLGA-NMe_3 (+15 mV) (Figure 3b). In the case of PLGA−PEG, they were between −30 and −40 mV. The NPs thus showed a general tendency to be negatively charged, probably due to the ∼10% remaining unreacted carboxy groups and deprotonation at the particle surface. Interestingly, uncharged PLGA−PEG gave smaller NPs for lower molecular weight, while charged PLGA polymers, especially bearing amine and sulfonate groups, gave smaller NPs for higher molecular weight (Figure 3a).

We then investigated whether this behavior as a function of the charge was limited to PLGA, or if it occurred more generally for different types of polymer backbones. We, hence, chose two other polymers, PCL and PMMA frequently used in biomedical applications. The former is, as PLGA, an aliphatic polyester, yet with a longer hydrocarbon chain between the ester groups, making it more hydrophobic and crystalline. PMMA is an acrylate polymer with an all carbon backbone characterized by a relatively high glass transition temperature >100 °C. For PCL the charged groups were introduced at the chain ends, though in this case both ends were modified. On the other hand, in PMMA the charged groups occurred at random positions along the chain. As for PLGA, the particle size of modified PMMA and PCL depended strongly on the nature of the polar group (Figure 4). For all three polymers the size of particles made from uncharged chains was largest, being typically above 100 nm. Carboxylate bearing polymers led to medium-sized particles between 60 and 100 nm. The TEM images of particles from uncharged and carboxy PMMA revealed a strong tendency of aggregate formation (this also made an analysis of the particle sizes difficult). Sulfonate and trimethylammonium-bearing polymers gave the smallest particles with sizes typically below 25 nm. The influence of one to two charged groups per chain thus outweighed largely the influence of the polymer type on the particle size. The only noticeable influence of the polymer type was that a minor population of larger particles (about 1% by volume of 250 nm particles) was systematically observed by DLS for PCL and its derivatives.

In the light of the small influence of the polymer type and molecular weight on particle size, the strong difference between sulfonate and carboxylate groups was surprising. We hypothesized that this might be due to the carboxylate group being protonated more readily, so that its (average) charge is reduced. Our earlier studies showed effectively that in phosphate buffer at pH 7.4, in which the carboxylate groups should be completely ionized, PLGA gives much smaller particles (∼40 nm)[15] than in Milli-Q water, reported

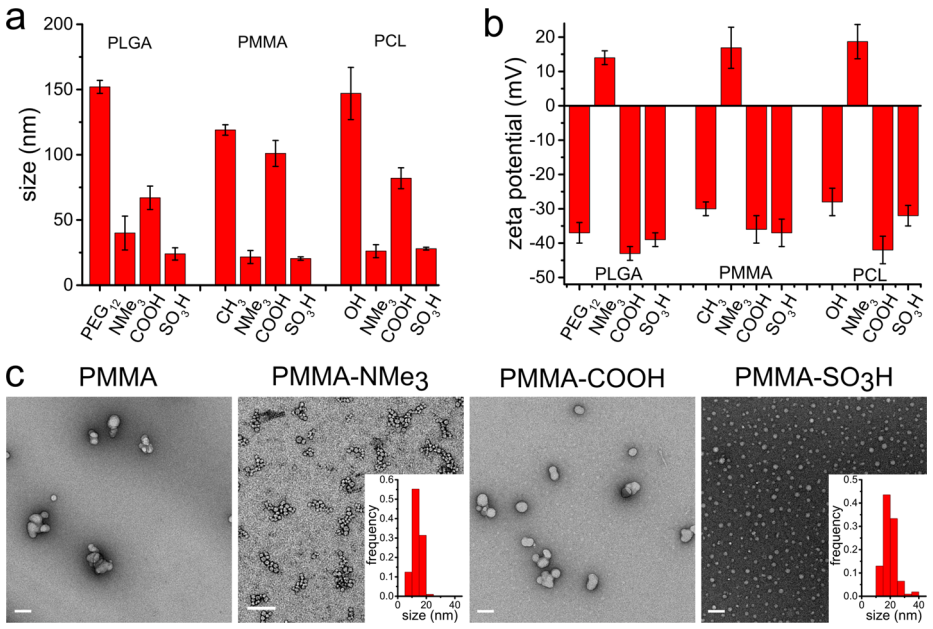

Figure 4. Influence of the end groups on size and zeta potential of nanoparticles from different polymers. (a) Size and (b) zeta potential of nanoparticles made from PLGA, PMMA, and PCL with different end or side groups as measured by dynamic light scattering. Nanoparticles were made using 2 mg mL^{-1} of PLGA (24 000) and 1 mg mL^{-1} for the other polymers in acetonitrile and water as the nonsolvent. (c) TEM images and size histograms of nanoparticles from PMMA, PMMA-NMe$_3$, PMMA-COOH, and PMMA-SO$_3$H. Values for the size are averages of volume distribution mean values; the error bars correspond to s.e.m. The scale bars correspond to 100 nm.

here. Nanoprecipitation of all three carboxylate bearing polymers in phosphate buffer at pH 7.4 showed indeed that the obtained particles were in the range of 40 to 55 nm as measured by DLS, and thus significantly smaller than in Milli-Q water (Figure 5). This indicated that the observed difference between sulfonate and carboxylate groups in water was effectively due to the carboxylate groups being not completely deprotonated and hence bearing fewer charges.

By introducing one to two charged groups per polymer chain we were hence able to reduce the size of the polymer NPs made by nanoprecipitation from over 100 to less than 25 nm. In order to decrease their size further, we then reduced the concentration of the polymer in acetonitrile for two representative examples: PLGA-COOH (M_n 7000) and PMMA-SO$_3$H. This led to very dilute particle solutions that could not be measured with high precision using DLS. Atomic force microscopy (AFM) and TEM were thus used instead. Decreasing the concentration did lead to a decrease of the particle size (Figure 6, Supporting Information Figure S2 and S3). For PLGA-COOH a decrease of the concentration down to 0.2 mg mL^{-1} decreased the mean diameter to about 14 nm. When the concentration was decreased further, no particles were detected by AFM. We could speculate that at too low concentrations the majority of the polymer was adsorbed on the surface of the sample tube. In the case of PMMA-SO$_3$H the particle diameter could be decreased to 14.5 nm when decreasing the polymer concentration to 0.2 mg mL^{-1}. When the concentration was further

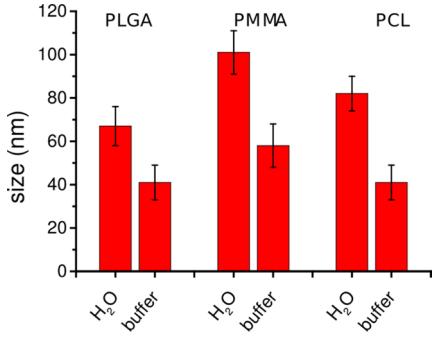

Figure 5. Influence of the nonsolvent on the particle size for carboxylate bearing polymers. Nanoparticles were made using solutions in acetonitrile (2 mg mL^{-1} for PLGA, 1 mg mL^{-1} for the other polymers) and either water or 20 mM phosphate buffer (pH of 7.4) as nonsolvent. Values are averages of volume distribution means; the error bars correspond to s.e.m.

reduced to 0.1 mg mL^{-1}, there was a further decrease of the size but only for a part of the NPs, while another part of the particles showed larger sizes of around 18 nm (Figure 6b, Supporting Information Figure S3), thus indicating that again the system was close to the limits of controlled particle formation.

Ultrasmall Nanocarriers as Fluorescent Nanoparticles. In the next step we verified whether charge controlled nanoprecipitation is suitable for encapsulating molecules in our ultrasmall nanoparticles. As a model system we chose a fluorescent dye which can be readily detected and should lead to dye-doped fluorescent nanoparticles—organic analogues of quantum

dots. The selected fluorescent dopant was a salt of a cationic dye, rhodamine B octadecyl ester (R18), with a bulky hydrophobic counterion, tetrakis(pentafluorophenyl)borate (F5-TPB) (Figure 1). In this system the hydrophobic counterion plays the role of a spacer that prevents aggregation-induced self-quenching of ionic dyes and facilitates their encapsulation.[15] Encapsulation is achieved simply by mixing the dye solution at the desired concentration with the polymer solution in acetonitrile followed by nanoprecipitation. Using ultracentrifugation, we were able to keep the ultrasmall PMMA-SO_3H NPs in suspension and to remove the nonencapsulated dye salt, which presumably formed large aggregates in water. Measuring the absorbance of the precipitation solutions showed that in the presence of polymer the dye concentration decreased by less than 10% upon ultracentrifugation (Supporting Information Figure S4). In the absence of the polymer, however, more than 95% of the dye salt were removed from the solution after ultracentrifugation. These measurements thus enabled evaluation of the degree of dye encapsulation in our nanoparticles. For the tested 0.5 to 5 wt % range the dye salt could be encapsulated into PMMA-SO_3H NPs with at least 90% efficiency (Figure 7a). Using a polymer concentration of 0.2 mg mL^{-1}, we could obtain NPs of 15 nm loaded with 5 wt % of R18/F5-TPB (Figure 7b). Fluorescence microscopy of these NPs immobilized on a surface revealed their excellent brightness. Indeed, the

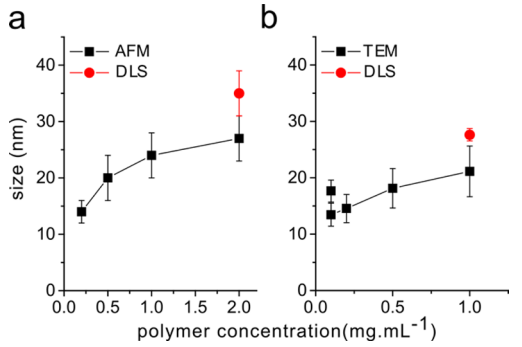

Figure 6. Influence of the polymer concentration on the particle size for (a) PLGA-COOH (M_n 7000) precipitated in 20 mM phosphate buffer (pH 7.4) and (b) PMMA-SO_3H precipitated in water. Values given for DLS are averages of volume distribution means; the error bars correspond to s.e.m. Values given for AFM and TEM are averages over at least 50 particles; the error bars correspond to the standard deviation.

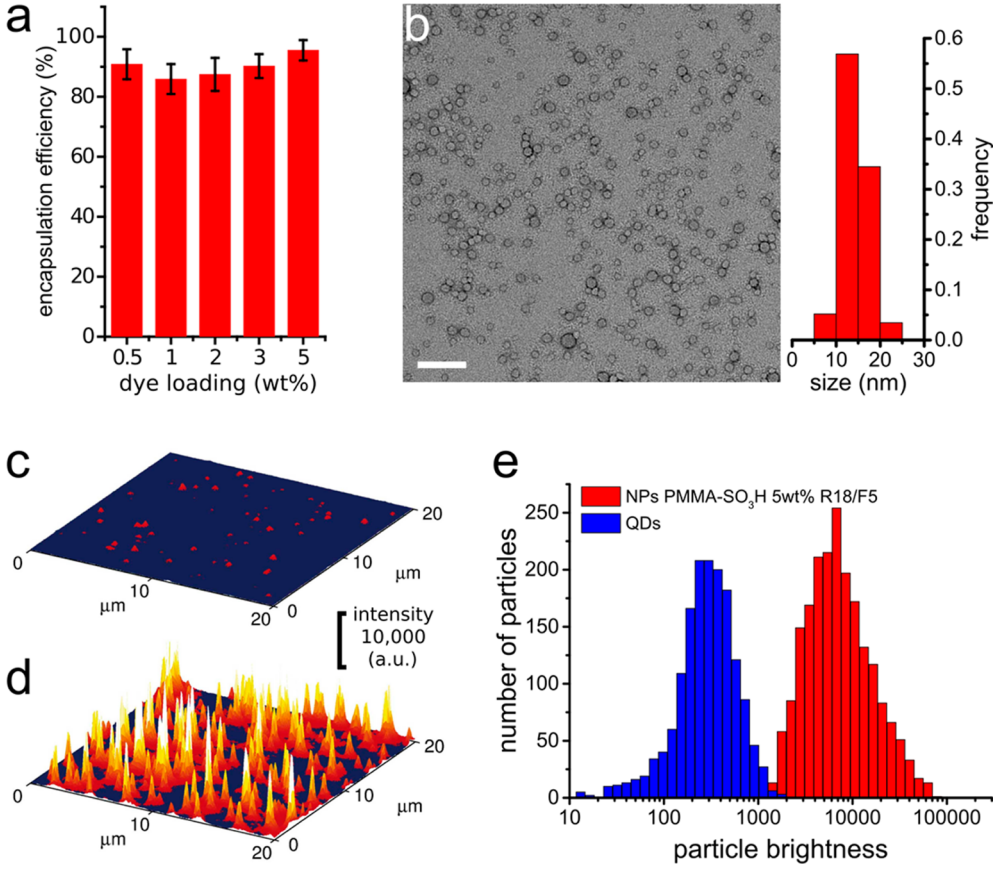

Figure 7. Dye-loaded fluorescent polymer nanoparticles. (a) Encapsulation efficiencies (estimated minimum percentage of the dye that was encapsulated in NPs) for R18/F5-TPB in PMMA-SO_3H nanoparticles. (b) TEM image and size histogram of the dye loaded PMMA-SO_3H nanoparticles. Scale bar 100 nm. Fluorescence microscopy images of (c) quantum dots (QDs, Qdot 585 Streptavidin Conjugates, Life Technologies) and (d) PMMA-SO_3H nanoparticles loaded with 5 wt % R18/F5-TPB obtained under the same conditions of illumination and recording, and (e) the corresponding distributions of single particle brightnesses.

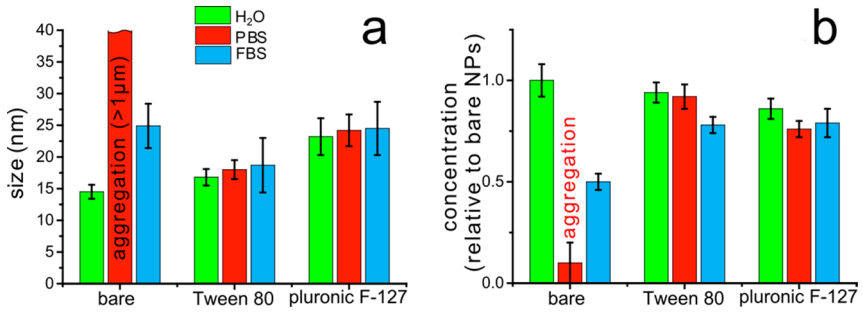

Figure 8. Stabilization of nanoparticles by surfactants. (a) Size and (b) concentration of PMMA-SO_3H NPs in Milli-Q-water, phosphate buffered saline (PBS), and 10 vol % fetal bovine serum (FBS) as measured by FCS. NPs were either used as made or treated with 0.05 mg mL^{-1} of Tween 80 or pluronic F-127. The NPs were obtained from 0.2 mg mL^{-1} solutions of PMMA-SO_3H. Error bars give the standard deviation over the 40 FCS measurements of a single sample.

dye loaded NPs were found to have a median single particle brightness of 6000 au and thus to be more than 10-fold brighter than commercial streptavidin bearing quantum dots of about the same size (15−20 nm according to the manufacturer) that had a median brightness of 400 au when imaged under the same conditions (Figure 7c,d,e).

Nanoparticle Stability and Interaction with Proteins. In order to be of practical use as nanocarriers, NPs have to be stable in biological media; *i.e.*, they should not aggregate at physiological salt concentrations and show minimal interaction with proteins. The influence of the medium on fluorescent NPs can be conveniently tested by fluorescence correlation spectroscopy (FCS), which allows measuring simultaneously their hydrodynamic diameter and concentration as well as estimating the dye release of NPs.[54,55] For our native 15 nm PMMA-SO_3H NPs loaded with R18/F5-TPB, FCS measurements showed a nearly complete precipitation of the NPs in phosphate buffered saline (PBS, Figure 8). In the presence of 10% fetal bovine serum (FBS) the hydrodynamic diameter of the NPs was observed to increase from 15 to 27 nm, while their concentration decreased by a factor close to 2. These NPs were hence not stable under physiological conditions. This was not really surprising as the average density of the sulfonate groups on their surface is one per 6.5 nm^2, and proteins adsorb even on like-charged NPs.[56] This means that the major part of the NP surface is occupied by relatively hydrophobic PMMA, which may favor adsorption of serum proteins and aggregation, when the repulsive forces of the sulfonate groups are screened by salt. On the other hand, this partially hydrophobic surface offers the possibility of surface modification using amphiphilic compounds. In order to reduce the effects of proteins and salts, amphiphiles containing PEG as the hydrophilic part are of particular interest.[18,31,57] According to FCS, addition of the nonionic surfactant Tween 80 (Polysorbate 80) and the amphiphilic block copolymer pluronic F-127 to our 15 nm NPs led only to a slight increase of their hydrodynamic diameter by 3 and 9 nm, respectively, indicating formation of a thin surfactant shell (Figure 8). Importantly, this surface modification made our NPs stable in PBS, as shown by the marginal changes in their size and concentration, in contrast to bare NPs (Figure 8). Furthermore, the particle size and concentrations remained stable after addition of 10% FBS, indicating that protein adsorption was largely inhibited after NP treatment with the surfactants. In addition, no increase in the concentration and no significant change of the particle brightness were observed (Figure 8b, Supporting Information Figure S6), indicating that no dye release occurred. Remarkably, the stabilization of NPs in physiological media was achieved at very low surfactant concentrations, namely 0.01−0.025 g/L (Supporting Information Figure S5), which are close to the critical micellar concentration (CMC) of Tween 80 (0.015 g/L),[58] but far below the CMC of pluronic F-127 (2.6−8.0 g/L).[59] Thus, a two-step modular approach, based on nanoprecipitation and further stabilization by a surfactant, allows obtaining sub-20-nm particles that are stable in physiological conditions and that show minimal interaction with proteins.

DISCUSSION

In the first part of this work we studied the influence of charged groups in PLGA, PCL, and PMMA polymers on the formation of particles through nanoprecipitation. Surprisingly, we found that the size of the resulting NPs was controlled by only one to two charged groups per polymer chain, while the nature of the polymer backbone and the molecular weight had a minor influence. Sulfonate and trimethylammonium groups, which are assumed to be fully charged under the used conditions, were the most effective for obtaining small particles. The size could be further decreased by decreasing the polymer concentration, which led to sub-15-nm particles. To better understand the origin of this phenomenon, the mechanism of particle formation has to be considered. In the case of low organic to aqueous phase ratios and low polymer concentrations, a nucleation and growth (or binodal) process is generally considered to prevail over spinodal decomposition, which consists in a rapid unmixing giving separate solid and liquid

phases.[41,45,46,60,61] Upon mixing of the organic and aqueous phase diffusion of the solvent into the aqueous phase (and *vice versa*) leads to a local supersaturation of the polymer. This supersaturation is the driving force for spontaneous nucleation and further growth of the so-formed primary particles. The final size of the particles then depends on the relative rates of nucleation, growth, and aggregation, with the smallest particles being formed at high nucleation rates, low growth rates, and very low aggregation rates.[45,61] The nucleation rate increases with decreasing nucleation parameter: $\gamma^3/\ln[S]^2$, where γ is the interfacial tension between the formed particles and the solution, and S is the supersaturation parameter. Turbidity measurements showed that the solubility in acetonitrile−water mixtures did not vary significantly for polymers having different end groups (Supporting Information Figure S7). As a consequence, for the identical concentrations used, the S value should not change drastically either. On the other hand, as the most hydrophilic groups are probably at the surface of the particles, the interfacial tension γ should be reduced strongly by charged groups and PEG. Thus, the presence of charged groups should reduce the nucleation parameter and hence increase the nucleation rate, leading to formation of smaller particles. The particle growth rate is proportional to the supersaturation S and the mass transfer coefficient k_m, corresponding to the rate constant of transport of mass to the growing particle. The latter decreases if charged polymers have to be brought to particles bearing the same charge. The decrease in the growth rate due to the presence of charges should then favor the formation of smaller particles. Finally, aggregation is prevented by a zeta potential more positive (negative) than +(−)30 mV. For negatively charged (and uncharged) polymers, the zeta potentials of the formed particles were indeed at least −30 mV, independently of their size. The zeta potential depends on the density of charges on the surface. Charged groups on the polymer thus help reach a potential necessary for preventing aggregation at smaller particle sizes and hence help stabilize small particles. This is in agreement with TEM micrographs that showed a tendency of aggregation notably for uncharged PMMA (Figure 4). The mechanism should be similar for the positively charged polymers, though the zeta potentials of their NPs were slightly smaller (15−20 mV). In summary, the presence of charged groups thus increases nucleation rates and decreases growth and aggregation rates. All three processes occurring during particle formation are hence pushed toward formation of smaller particles, which can explain the strong influence of the presence of one to two charged groups per polymer chain. The observed smaller particle size for higher molecular weight in case of charged PLGAs can be explained by a kinetic control of the growth step, where the mass transfer coefficient k_m decreases with increasing molecular weight. In the presence of neutral PEG groups a larger influence of thermodynamic factors on the control of the particle growth is assumed. Stabilization and repulsion is then reached through optimization of the density of PEG on the surface, and for lower polymer molecular weight a given density is reached for smaller particle sizes.

A remarkable feature of the NPs prepared by charge-controlled nanoprecipitation is the nearly quantitative encapsulation of organic dyes. Moreover, according to the FCS data, no burst release of the dye was observed in a biological medium, PBS with 10% serum, which is an excellent recipient of apolar molecules. In contrast, small micellar NPs prepared from block copolymers present relatively low encapsulation efficiency[62,63] together with significant burst release.[34−38] This is probably related to the dynamic equilibrium between the micelles and individual polymer molecules, due to their partial solubility in aqueous solution. In contrast, the polymers used here for the preparation of NPs through charge-controlled nanoprecipitation have only a minimal number of charges and thus a very low water solubility (Supporting Information Figure S7). The latter should favor the stable and nearly quantitative encapsulation of hydrophobic molecules inside these particles and the undetectable burst release in serum. It should be noted, that the choice of the hydrophobic molecule for encapsulation is also important. As we showed earlier,[15] efficient encapsulation of cationic dye R18 can be achieved using bulky hydrophobic counterions that make the dye more hydrophobic and prevent it from accumulating at the negatively charged particle surface.

The third important feature is the effective stabilization of our charged NPs by remarkably small concentrations of surfactants, which are significantly lower than those normally used in nanoprecipitation.[64−66] Tween and pluronic amphiphiles are known to stabilize uncoated NPs after their preparation.[67,68] Here we showed using FCS that the surfactant shell is only 1.5 and 4.5 nm thick for Tween 80 and pluronic F-127, respectively. This thickness is smaller than the hydrodynamic radius of 3−5 nm[69] and 10−12 nm[70] of the micelles formed by Tween 80 and pluronic F-127, respectively. Therefore, we can speculate that surfactants at these low concentrations underwent a strong adsorption of their alkyl chains at the hydrophobic sites of the NPs without forming a lipid monolayer, and thus gave an ultrathin protective shell (Figure 9). Remarkably, this shell was sufficiently stable to prevent particle aggregation in salts and protect the NPs from adsorption of serum proteins. Some reports showed that surfactants are not absolutely necessary for preparation of polyester NPs.[71,72] According to our data, the surfactants are indeed not necessary for particle preparation, but they are important as "corona" that

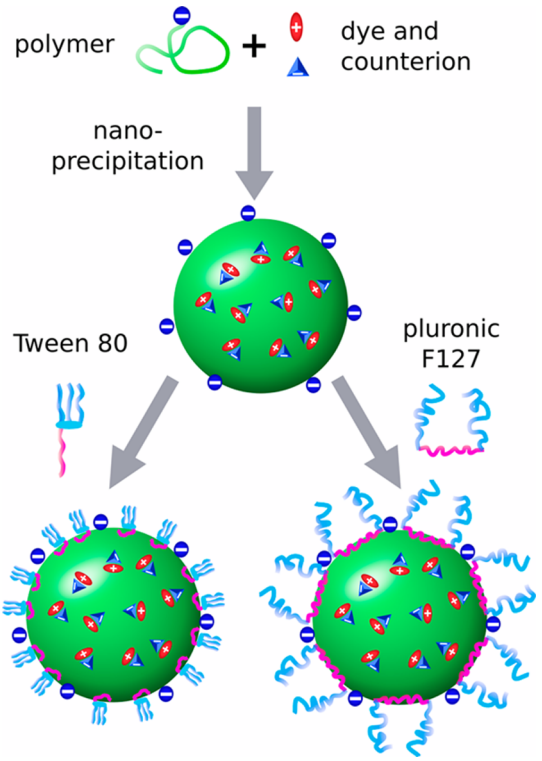

Figure 9. Scheme of the modular two-steps approach used to prepare stable nanocarriers through charge-controlled nanoprecipitation. A polymer bearing a charged group is mixed with a cargo molecule (the dye salt) in an organic solvent and precipitated in water. The resulting particles are stabilized in a second step using Tween 80 or pluronic F-127.

can be added after particle preparation and serve to protect the NPs from aggregation and nonspecific interactions. Thus, we propose a two-step modular approach for the synthesis of ultrasmall nanoparticles, consisting in (1) charge controlled nanoprecipitation in low-salt conditions, followed by (2) stabilization of the particle surface by a surfactant (Figure 9). This highly flexible approach can be, in principle, extended to other polymers and other types of surface modification.

CONCLUSION

Ultrasmall nanoparticles are of special interest as nanocarriers of contrast agents and drugs. Here we have developed charge controlled nanoprecipiation as a modular approach to the assembly of ultrasmall stable polymeric nanocarriers. We showed that the presence of only one to two charged groups per polymer chain can strongly reduce the size of polymer nanoparticles made by nanoprecipitation. This concept works with negatively charged groups, such as carboxyl and sulfonate as well as with positively charged trimethylammonium. Its success with three quite different types of polymers (PLGA, PCL, and PMMA) suggests its general usefulness for the preparation of polymer nanocarriers. Moreover, the particle size can be further decreased to less than 15 nm by minimizing the concentration of polymer in the solvent used for nanoprecipitation. We further showed that even very small nanoparticles of 15 nm size preserve the capacity to encapsulate efficiently large amounts of ionic dyes with bulky counterions, which generates polymer nanoparticles 10-fold brighter than quantum dots of the same size. These nanocarriers could be stabilized by surface modification using PEG-containing amphiphiles, leading to particles that show minimal interactions with proteins. This straightforward and modular route could become a general approach for the preparation of ultrasmall polymer nanoparticles as nanocarriers of contrast agents and drugs.

MATERIALS AND METHODS

Materials. Poly(D,L-lactide-*co*-glycolide) (PLGA noted here as PLGA-COOH, lactide 50 mol %, glycolide 50 mol %, acid terminated, M_n 24 000, PDI 1.7, and M_n 8800, PDI 1.7), polycaprolactone (α,ω-dihydroxy functional, M_n ~10 000, M_w ~14 000), poly(methyl methacrylate) (PMMA, M_w 120 000), poly(methyl methacrylate-*co*-methacrylic acid) (PMMAMA noted here as PMMA-COOH, 1,3% methacrylic acid, M_n ~15 000, M_w ~34 000), *N*,*N*,*N*′,*N*′-tetramethyl-*O*-(1*H*-benzotriazol-1-yl)uronium hexafluorophosphate (HBTU, >98.0%), 1-hydroxybenzotriazole hydrate (HOBt, >99.0%), *N*,*N*-diisopropylethylamine (DIPEA, 99,5%), acetonitrile (anhydrous, 99.8%), dichloromethane (anhydrous, >99.8%), (2-aminoethyl) trimethylammonium chloride hydrochloride (99%), rhodamine B octadecyl ester perchlorate (>98.0%), lithium tetrakis(pentafluorophenyl)borate ethyl etherate, Tween 80, pluronic F-127 were purchased from Sigma-Aldrich. Amine terminated polyethylene glycols (H_2N-PEG(8)N_3, H_2N-PEG(12)N_3, H_2N-PEG(24)N_3) were purchased from Iris Biotech. *N*,*N*′-dimethylformamide (absolute >99.8%) and succinic anhydride were purchased from AlfaAesar. 2-Aminoethanesulfonic acid (taurine, >98%) was obtained from TCI. Sodium phosphate monobasic (>99.0%, Sigma-Aldrich) and sodium phosphate dibasic dihydrate (>99.0%, Sigma-Aldrich) were used to prepare 20 mM phosphate buffer solutions at pH 7.4; tris(hydroxymethyl)aminomethane (Tris base, >99.8%, Sigma-Aldrich) and HCl (1 M) were used to prepare 20 mM Tris buffer with a pH of 7.4. Milli-Q water (Millipore) was used in all experiments. Qdot 585 Streptavidin Conjugates were purchased from Life-Technologies.

Synthesis. *Rhodamine B Octadecyl Ester Tetrakis(pentafluorophenyl)borate (R18/F5-TPB).* Title compound was synthesized by ion exchange and purified by column chromatography as described previously.[15]

PLGA—PEG. Given is, as an example, the procedure for PLGA—PEG_{24} 24 000: 40 mg of PLGA (0.0017 mmol, 1 equiv of COOH) were dissolved in anhydrous dichloromethane (2 mL). To this solution DIPEA (3 μL, 0.017 mmol, 10 equiv), HOBt (0.55 mg, 0.004 mmol, 2.4 equiv) and HBTU (1.27 mg, 0.003 mmol, 2 equiv) were added as solutions in anhydrous dimethylformamide (total of 1 mL) under argon. 3.7 mg of NH_2-PEG(23)-N_3 (0.003 mmol, 2 equiv) were dissolved in 0.3 mL of DMF and added to the reaction mixture. After stirring for 18 h at room temperature, part of the solvent was evaporated at 40 °C under reduced pressure. The obtained solution was precipitated in methanol. The precipitate was washed with methanol, redissolved in acetonitrile, and reprecipitated twice in methanol. After drying under a vacuum, 27 mg of a white solid were obtained (yield 65%). ^{1}H NMR (400 MHz, $CDCl_3$): δ/ppm 5.3—5.1 (m, 1 H), 4.9—4.6 (m, 2 H), 4.30 (m, 0.011 H), 3.64 (m, 0.4 H), 3.47

(br, 0.016 H), 3.38 (t, 0.011 H), 1.8−1.4 (m, 3 H). Degree of modification 86%.

PLGA−PEG_{12} 24 000: 32 mg obtained (yield 79%). Degree of modification 96%.

PLGA−PEG_8 24 000: 15 mg obtained (yield 75%). Degree of modification 94%.

PLGA−PEG_{24} 7000: 42 mg obtained (yield 73%). Degree of modification 67%.

PLGA−PEG_{12} 7000: 35 mg obtained (yield 65%). Degree of modification 69%.

PLGA−PEG_8 7000: 17 mg obtained (yield 80%). Degree of modification 66%.

PCL-COOH. The PCL (244 mg, 0.0244 mmol, 2 equiv of OH) was dissolved in anhydrous acetonitrile (4,8 mL) at 40 °C. Succinic anhydride (12.3 mg, 0.123 mmol, 5 equiv) and DIPEA (50 μL, 0.302 mmol) were added under stirring. The mixture was stirred at 45 °C under argon atmosphere for 18 h. The solvent was evaporated under reduced pressure. After redissolution in a small amount of acetonitrile the solution was precipitated in methanol. The precipitate was washed with methanol, redissolved in acetonitrile, and reprecipitated twice in methanol. After drying under a vacuum, 102 mg of a white solid were obtained (yield 41%). ^{1}H NMR (400 MHz, $CDCl_3$): δ/ppm 4.05 (t, 2 H), 3.7−3.6 (m, 0.09 H), 2.63 (m, 0.08 H), 2.30 (t, 2 H), 1.64 (m, 4 H), 1.38 (m, 2 H). Degree of modification 80%.

Trimethylammonium Bearing Polymers. The basic procedure was the same for all polymers except that PCL-COOH and PMMA-COOH were reacted at 40 °C; given are the quantities used for PLGA-NMe_3 24 000: The PLGA (40 mg, 0.0017 mmol, 1 equiv of COOH) was dissolved in anhydrous dichloromethane (3 mL). 2-(Aminoethyl)trimethylammonium chloride hydrochloride (3 mg, 0.017 mmol, 10 equiv), DIPEA (25 μL, 0.15 mmol, 88 equiv), HOBt (2.3 mg, 0.017 mmol, 10 equiv) and HBTU (6.4 mg, 0.017 mmol, 10 equiv) were dissolved in anhydrous dimethylformamide (total of 2 mL) and added to the PLGA solution under argon. The mixture was stirred for 20 h at room temperature. After evaporating part of the solvent at 40 °C under reduced pressure, the solution was precipitated in methanol. The precipitate was washed with methanol, redissolved in acetonitrile, and reprecipitated twice in methanol. After drying under a vacuum, 25 mg of a white solid were obtained (yield 63%). ^{1}H NMR (400 MHz, $CDCl_3$): δ/ppm 5.3−5.1 (m, 1 H), 4.9−4.6 (m, 2H), 4.27 (m, 0.013 H), 3.76 (m, 0.009 H), 3.64 (br, 0.008 H), 3.26 (br, 0.043 H), 1.8−1.4 (m, 3 H).

PLGA-NMe_3 7000 18 mg were obtained (yield 45%). Degree of modification 88%.

PCL-NMe_3: 12 mg obtained (yield 42%). Degree of modification 70%.

PMMA-NMe_3: 82 mg obtained (yield 55%). Degree of modification 60%.

Sulfonate Bearing Polymers. The same procedure was used for the introduction of sulfonate groups into all polymers starting from the corresponding carboxyl bearing polymers. Given is, as an example, the detailed procedure for PLGA-SO_3H 24 000: The PLGA (102 mg, 0,0042 mmol, 1 equiv of COOH) was dissolved in anhydrous DMF (1.5 mL) under argon. Taurine (5.2 mg, 0.042 mmol, 10 equiv) and DIPEA (30 μL, 0.18 mmol) were added to the solution, followed by the addition of HOBt (4.6 mg, 0.034 mmol, 8 equiv) and HBTU (12.5 mg, 0.033 mmol, 8 equiv). The mixture was stirred under argon for 20 h at 40 °C. After evaporating part of the solvent at 40 °C under reduced pressure, the solution was precipitated in methanol. The precipitate was washed with methanol, redissolved in acetonitrile, and reprecipitated twice in methanol. After drying under a vacuum, 57 mg of a white solid were obtained (yield 55%). ^{1}H NMR (400 MHz, $CDCl_3$): δ/ppm 5.3−5.1 (m, 1 H), 4.9−4.6 (m, 2 H), 4.30 (m, 0.011 H), 3.80−3.65 (m, 0.020 H), 3.10 (0.006 H), 2.98 (m, 0.010 H), 1.8−1.4 (m, 3 H). Degree of modification 91%.

PLGA-SO_3H 7000: 75 mg obtained (yield 74%). Degree of modification 86%.

PCL-SO_3H: 157 mg obtained (yield 62%). Degree of modification 78%.

PMMA-SO_3H: 114 mg obtained (yield 78%). Degree of modification 85%.

Nanoparticle Preparation. Stock solutions of the polymers in acetonitrile were prepared at a concentration of 10 mg mL^{-1}. These solutions were then diluted with acetonitrile to the desired concentration (between 0.05 and 2 mg mL^{-1}). 50 μL of the polymer solutions were then added quickly using a micropipette and under shaking (Thermomixer comfort, Eppendorf, 1000 rpm) to 450 μL of water or buffer. PLGA and PMMA based nanoparticles were prepared at 21 °C, PCL nanoparticles were prepared at 27 °C. The particle solution was then quickly diluted 5-fold with the same buffer. For preparation of fluorescent nanoparticles, different concentrations of R18/F5-TPB (0.5 to 5 wt % relative to the polymer) were added to the acetonitrile solution used for particle preparation, and the particles were prepared as described above. For stabilization of NPs, different amounts of 1 or 0.1 mg mL^{-1} solutions of Tween 80 or pluronic F-127 were added under stirring to the NP solutions.

Nanoparticle Characterization. *Dynamic Light Scattering.* measurements for the determination of the size, size distribution, and zeta-potential of the nanoparticles were performed on a Zetasizer Nano series DTS 1060 (Malvern Instruments S.A.). The mean value of the diameter of the size distribution per volume was used for analysis. Each sample was measured three times and each condition was tested at least in triplicate in independent measurements. The errors (bars) are given as the standard error of the mean.

Electron Microscopy. Five microliters of the particle solution were deposited onto carbon-coated copper−rhodium electron microscopy grids that were used either as obtained or following an air or amylamine glow-discharge. The grids were then treated for 1 min with a 2% uranyl acetate solution for staining. They were then observed with a Philips CM120 transmission electron microscope equipped with a LaB_6 filament and operating at 100 kV. Areas covered with nanoparticles of interest were recorded at different magnifications on a Peltier cooled CCD camera (Model 794, Gatan, Pleasanton, CA). Image analysis was performed using the Fiji software.

Atomic Force Microscopy. AFM measurements were performed using a commercial instrument (Solver Pro-M, NT-MDT, Moscow) in the tapping mode in liquid phase. The cantilever used were CSG01 (NT-MDT, Moscow) with a typical spring constant of 0.06 N/m and a resonance frequency of 11 kHz. Images were acquired with a resolution of 512 × 512 points and a scan rate of 1 Hz. The samples were prepared using 100 μL deposed on cleaved mica coated with polyethylenimine (PEI) as described below. The measurements were performed 10 min after sample preparation. Analysis of particle populations was done using Gwydion 2.31 and Origin 8.0.

Encapsulation Efficiency. Eight milliliters of NP solution (at a polymer concentration of 0.02 mg μL^{-1} and containing between 0.5 and 5 wt % R18/F5-TPB) were ultracentrifuged using polycarbonate thick-wall centrifuge tubes (Beckman Coulter Inc.) in a Beckman Coulter Ultracentrifuge using a Ti90 rotor at 125000*g* for 12 min at 23 °C. Absorbances at 555 nm before and after ultracentrifugation were measured in the supernatant. The same procedure was applied to the same amounts of dye in water without the polymer. The encapsulation efficiency was calculated from the percentage of absorbance remaining after ultracentrifugation. To take into account the nonencapsulated dye that might not be removed by ultracentrifugation, the percentage of remaining absorbance in the absence of polymer after ultracentrifugation was subtracted: encapsulation efficiency = $A_{NP}^{after}/A_{NP}^{before} - A_{dye}^{after}/A_{dye}^{before}$.

Fluorescence Microscopy. For single particle fluorescence microscopy measurements, the NPs were immobilized on glass surfaces on which a polyethylenimine (PEI) layer was initially adsorbed. The solutions of NPs were diluted to a particle concentration of about 6 pM with water or buffer (particle concentration before the dilution was estimated by fluorescence correlation spectroscopy, see below). 400 μL of these solutions per cm^2 were then brought in contact with the PEI covered glass for 15 min, followed by extensive rinsing with Milli-Q-water. The surfaces were left in Milli-Q water during microscopy. Quantum dots (Qdot 585 Streptavidin Conjugates, life technologies) at 6 pM concentration were immobilized and imaged in the same way as the NPs.

Single particle measurements were performed in the TIRF (Total Internal Reflection Fluorescence) mode on a homemade wide-field setup based on an Olympus IX-71 microscope with an oil immersion objective (NA = 1.49, 100×). A DPPS (Cobolt) continuous wave (CW) laser emitting at 532 nm was used for excitation. The laser intensity was set to 4.5 W cm^{-2} by using a polarizer and a half-wave plate (532 nm). The fluorescence signal was recorded with an EMCCD (ImagEM Hamamatsu) using an exposure of 30 ms per image frame. Single particle analysis was performed using the Fiji software as described previously.[15,73] Briefly, particle locations were detected through a Fiji routine applied to a projection (maximum intensity) of 100 frames. The mean intensities of circular regions of interest with a diameter of 5 pixels around the found particle locations were then measured. Background subtraction was then achieved by measuring the mean intensities in circular bands around the circular regions of interest and subtracting them. Three image sequences (55 μm × 55 μm) per condition were analyzed with, on average, 680 and 530 particles per image for PMMA-SO_3H NPs and QDs, respectively.

Fluorescence Correlation Spectroscopy (FCS) and NP Stability. FCS measurements were performed on a two-photon platform including an Olympus IX70 inverted microscope, as described previously.[55,74] Two-photon excitation at 830 nm (10 mW laser output power) was provided by an InSight DeepSee laser (Spectra Physics). The measurements were carried out in 96-well optical-bottom plates, using 125 μL per well. The focal spot was set about 20 μm above the cover- slip. The normalized autocorrelation function, $G(\tau)$, was calculated online using an ALV-5000E correlator (ALV, Germany) from the fluorescence fluctuations, $\delta F(t)$, by $G(\tau) = \langle \delta F(t)\delta F(t+\tau)\rangle / \langle F(t)\rangle^2$ where $\langle F(t)\rangle$ is the mean fluorescence signal and τ is the lag time. Assuming that NPs diffuse freely in a Gaussian excitation volume, the correlation function, $G(\tau)$, calculated from the fluorescence fluctuations was fitted according to[54]

$$G(\tau) = \frac{1}{N}\left(1+\frac{\tau}{\tau_d}\right)^{-2}\left(1+\frac{1}{S^2}\frac{\tau}{\tau_d}\right)^{-1/2}$$

where τ_d is the diffusion time, N is the mean number of fluorescent species within the two-photon excitation volume, and S is the ratio between the axial and lateral radii of the excitation volume. The excitation volume is about 0.34 fL and S is about 3 to 4. The typical data recording time was 5 min, using freshly prepared NPs without further dilution. The measurements were done with respect to 6-carboxy- tetramethylrhodamine (TMR from Sigma-Aldrich) in water, used as a reference. The hydrodynamic diameter, d, of NPs was calculated as $d_{NPs} = \tau_{d(NPs)} / \tau_{d(TMR)} \times d_{TMR}$, where d_{TMR} is the hydrodynamic diameter of TMR (1.0 nm). The concentration of NPs was calculated from the number of species by $C(NPs) = N(NPs)/N(TMR) \times C(TMR)$, using a TMR concentration of 140 nM.

NP stability in PBS was tested by adding 10 vol % of 10-fold concentrated PBS to the solutions of the corresponding NPs containing 1 wt % of R18/F5-TPB and measuring the hydrodynamic diameter and concentration. Interaction with 10 vol % fetal bovine serum was tested in the same way.

Conflict of Interest: The authors declare no competing financial interest.

Acknowledgment. The authors thank C. Ruhlmann for help with electron microscopy and C. Antheaume and J. Viéville for help with NMR spectroscopy. This work was supported by ANR JCJC (ANR-11-JS07-014-01), CNRS, and the University of Strasbourg.

Supporting Information Available: Includes additional NMR spectra, AFM and additional TEM images, data on encapsulation efficiencies, NP stability, and polymer solubilities. This material is available free of charge *via* the Internet at http://pubs.acs.org.

REFERENCES AND NOTES

1. Panyam, J.; Labhasetwar, V. Biodegradable Nanoparticles for Drug and Gene Delivery to Cells and Tissue. *Adv. Drug Delivery Rev.* **2003**, *55*, 329–347.
2. Danhier, F.; Ansorena, E.; Silva, J. M.; Coco, R.; Le Breton, A.; Preat, V. PLGA-Based Nanoparticles: An Overview of Biomedical Applications. *J. Controlled Release* **2012**, *161*, 505–522.
3. Kumari, A.; Yadav, S. K.; Yadav, S. C. Biodegradable Polymeric Nanoparticles Based Drug Delivery Systems. *Colloids Surf., B* **2010**, *75*, 1–18.
4. Kulkarni, S. A.; Feng, S.-S. Effects of Particle Size and Surface Modification on Cellular Uptake and Biodistribution of Polymeric Nanoparticles for Drug Delivery. *Pharm. Res.* **2013**, *30*, 2512–2522.
5. Choi, H. S.; Liu, W.; Misra, P.; Tanaka, E.; Zimmer, J. P.; Ipe, B. I.; Bawendi, M. G.; Frangioni, J. V. Renal Clearance of Nanoparticles. *Nat. Biotechnol.* **2007**, *25*, 1165–1170.
6. Huo, S.; Ma, H.; Huang, K.; Liu, J.; Wei, T.; Jin, S.; Zhang, J.; He, S.; Liang, X.-J. Superior Penetration and Retention Behavior of 50 nm Gold Nanoparticles in Tumors. *Cancer Res.* **2013**, *73*, 319–330.
7. Cabral, H.; Matsumoto, Y.; Mizuno, K.; Chen, Q.; Murakami, M.; Kimura, M.; Terada, Y.; Kano, M. R.; Miyazono, K.; Uesaka, M.; *et al.* Accumulation of Sub-100 nm Polymeric Micelles in Poorly Permeable Tumours Depends on Size. *Nat. Nanotechnol.* **2011**, *6*, 815–823.
8. Wong, C.; Stylianopoulos, T.; Cui, J.; Martin, J.; Chauhan, V. P.; Jiang, W.; Popović, Z.; Jain, R. K.; Bawendi, M. G.; Fukumura, D. Multistage Nanoparticle Delivery System for Deep Penetration into Tumor Tissue. *Proc. Natl. Acad. Sci. U. S. A.* **2011**, *108*, 2426–2431.
9. Rosi, N. L.; Giljohann, D. A.; Thaxton, C. S.; Lytton-Jean, A. K. R.; Han, M. S.; Mirkin, C. A. Oligonucleotide-Modified Gold Nanoparticles for Intracellular Gene Regulation. *Science* **2006**, *312*, 1027–1030.
10. Verma, A.; Uzun, O.; Hu, Y.; Hu, Y.; Han, H.-S.; Watson, N.; Chen, S.; Irvine, D. J.; Stellacci, F. Surface-Structure-Regulated Cell-Membrane Penetration by Monolayer-Protected Nanoparticles. *Nat. Mater.* **2008**, *7*, 588–595.
11. Sahay, G.; Alakhova, D. Y.; Kabanov, A. V. Endocytosis of Nanomedicines. *J. Controlled Release* **2010**, *145*, 182–195.
12. Maria Coto-Garcia, A.; Sotelo-Gonzalez, E.; Teresa Fernandez-Argueelles, M.; Pereiro, R.; Costa-Fernandez, J. M.; Sanz-Medel, A. Nanoparticles as Fluorescent Labels for Optical Imaging and Sensing in Genomics and Proteomics. *Anal. Bioanal. Chem.* **2011**, *399*, 29–42.
13. Wagh, A.; Qian, S. Y.; Law, B. Development of Biocompatible Polymeric Nanoparticles for *in Vivo* NIR and FRET Imaging. *Bioconjugate Chem.* **2012**, *23*, 981–992.
14. Wagh, A.; Jyoti, F.; Mallik, S.; Qian, S.; Leclerc, E.; Law, B. Polymeric Nanoparticles with Sequential and Multiple FRET Cascade Mechanisms for Multicolor and Multiplexed Imaging. *Small* **2013**, *9*, 2129–2139.
15. Reisch, A.; Didier, P.; Richert, L.; Oncul, S.; Arntz, Y.; Mély, Y.; Klymchenko, A. S. Collective Fluorescence Switching of Counterion-Assembled Dyes in Polymer Nanoparticles. *Nat. Commun.* **2014**, *5*, 4089.
16. Michalet, X.; Pinaud, F. F.; Bentolila, L. A.; Tsay, J. M.; Doose, S.; Li, J. J.; Sundaresan, G.; Wu, A. M.; Gambhir, S. S.; Weiss, S. Quantum Dots for Live Cells, *in Vivo* Imaging, and Diagnostics. *Science* **2005**, *307*, 538–544.
17. Wang, M.; Abbineni, G.; Clevenger, A.; Mao, C.; Xu, S. Upconversion Nanoparticles: Synthesis, Surface Modification and Biological Applications. *Nanomedicine* **2011**, *7*, 710–729.
18. Howes, P. D.; Chandrawati, R.; Stevens, M. M. Colloidal Nanoparticles as Advanced Biological Sensors. *Science* **2014**, *346*, 1247390.
19. Li, Z.; Sun, Q.; Zhu, Y.; Tan, B.; Xu, Z. P.; Dou, S. X. Ultra-Small Fluorescent Inorganic Nanoparticles for Bioimaging. *J. Mater. Chem. B* **2014**, *2*, 2793–2818.
20. Cognet, L.; Leduc, C.; Lounis, B. Advances in Live-Cell Single-Particle Tracking and Dynamic Super-Resolution Imaging. *Curr. Opin. Chem. Biol.* **2014**, *20*, 78–85.
21. Wang, X.; Stolwijk, J. A.; Lang, T.; Sperber, M.; Meier, R. J.; Wegener, J.; Wolfbeis, O. S. Ultra-Small, Highly Stable, and Sensitive Dual Nanosensors for Imaging Intracellular Oxygen and pH in Cytosol. *J. Am. Chem. Soc.* **2012**, *134*, 17011–17014.

22. Zhang, L.; Chan, J. M.; Gu, F. X.; Rhee, J.-W.; Wang, A. Z.; Radovic-Moreno, A. F.; Alexis, F.; Langer, R.; Farokhzad, O. C. Self-Assembled Lipid−Polymer Hybrid Nanoparticles: A Robust Drug Delivery Platform. *ACS Nano* **2008**, *2*, 1696–1702.
23. Santander-Ortega, M. J.; Jódar-Reyes, A. B.; Csaba, N.; Bastos-González, D.; Ortega-Vinuesa, J. L. Colloidal Stability of Pluronic F68-Coated PLGA Nanoparticles: A Variety of Stabilisation Mechanisms. *J. Colloid Interface Sci.* **2006**, *302*, 522–529.
24. Gillich, T.; Acikgöz, C.; Isa, L.; Schlüter, A. D.; Spencer, N. D.; Textor, M. PEG-Stabilized Core−Shell Nanoparticles: Impact of Linear *versus* Dendritic Polymer Shell Architecture on Colloidal Properties and the Reversibility of Temperature-Induced Aggregation. *ACS Nano* **2012**, *7*, 316–329.
25. Rao, J. P.; Geckeler, K. E. Polymer Nanoparticles: Preparation Techniques and Size-Control Parameters. *Prog. Polym. Sci.* **2011**, *36*, 887–913.
26. Landfester, K. Miniemulsion Polymerization and the Structure of Polymer and Hybrid Nanoparticles. *Angew. Chem., Int. Ed.* **2009**, *48*, 4488–4507.
27. Allen, C.; Maysinger, D.; Eisenberg, A. Nano-Engineering Block Copolymer Aggregates for Drug Delivery. *Colloids Surf., B* **1999**, *16*, 3–27.
28. Kataoka, K.; Harada, A.; Nagasaki, Y. Block Copolymer Micelles for Drug Delivery: Design, Characterization and Biological Significance. *Adv. Drug Delivery Rev.* **2001**, *47*, 113–131.
29. Riess, G. Micellization of Block Copolymers. *Prog. Polym. Sci.* **2003**, *28*, 1107–1170.
30. Gohy, J.-F.; Willet, N.; Varshney, S.; Zhang, J.-X.; Jérôme, R. Core−Shell−Corona Micelles with a Responsive Shell. *Angew. Chem., Int. Ed.* **2001**, *40*, 3214–3216.
31. Otsuka, H.; Nagasaki, Y.; Kataoka, K. PEGylated Nanoparticles for Biological and Pharmaceutical Applications. *Adv. Drug Delivery Rev.* **2012**, *64* (Supplement), 246–255.
32. Nagarajan, R.; Ganesh, K. Block Copolymer Self-assembly in Selective Solvents: Spherical Micelles with Segregated Cores. *J. Chem. Phys.* **1989**, *90*, 5843–5856.
33. Mortensen, K.; Brown, W. Poly(ethylene Oxide)-Poly(propylene Oxide)-Poly(ethylene Oxide) Triblock Copolymers in Aqueous Solution. The Influence of Relative Block Size. *Macromolecules* **1993**, *26*, 4128–4135.
34. Zou, P.; Chen, H. W.; Paholak, H. J.; Sun, D. X. Burst Release of Lipophilic Drugs from Poly (Ethylene Oxide)- B-Polystyrene Micelles Is Not Caused by Micelle Disassembly. *J. Tumor* **2013**, *1*, 7–15.
35. Bae, Y. H.; Yin, H. Stability Issues of Polymeric Micelles. *J. Controlled Release* **2008**, *131*, 2–4.
36. Chen, H.; Kim, S.; He, W.; Wang, H.; Low, P. S.; Park, K.; Cheng, J.-X. Fast Release of Lipophilic Agents from Circulating PEG-PDLLA Micelles Revealed by *in Vivo* Förster Resonance Energy Transfer Imaging. *Langmuir* **2008**, *24*, 5213–5217.
37. Chen, H.; Kim, S.; Li, L.; Wang, S.; Park, K.; Cheng, J.-X. Release of Hydrophobic Molecules from Polymer Micelles into Cell Membranes Revealed by Förster Resonance Energy Transfer Imaging. *Proc. Natl. Acad. Sci. U. S. A.* **2008**, *105*, 6596–6601.
38. Zhao, X.; Poon, Z.; Engler, A. C.; Bonner, D. K.; Hammond, P. T. Enhanced Stability of Polymeric Micelles Based on Postfunctionalized Poly(ethylene Glycol)-B-Poly(γ-Propargyl L-Glutamate): The Substituent Effect. *Biomacromolecules* **2012**, *13*, 1315–1322.
39. Schulz, A.; Jaksch, S.; Schubel, R.; Wegener, E.; Di, Z.; Han, Y.; Meister, A.; Kressler, J.; Kabanov, A. V.; Luxenhofer, R.; *et al.* Drug-Induced Morphology Switch in Drug Delivery Systems Based on Poly(2-Oxazoline)s. *ACS Nano* **2014**, *8*, 2686–2696.
40. Fessi, H.; Puisieux, F.; Devissaguet, J. P.; Ammoury, N.; Benita, S. Nanocapsule Formation by Interfacial Polymer Deposition Following Solvent Displacement. *Int. J. Pharm.* **1989**, *55*, R1–R4.
41. Mora-Huertas, C. E.; Fessi, H.; Elaissari, A. Influence of Process and Formulation Parameters on the Formation of Submicron Particles by Solvent Displacement and Emulsification−Diffusion Methods: Critical Comparison. *Adv. Colloid Interface Sci.* **2011**, *163*, 90–122.
42. Govender, T.; Stolnik, S.; Garnett, M. C.; Illum, L.; Davis, S. S. PLGA Nanoparticles Prepared by Nanoprecipitation: Drug Loading and Release Studies of a Water Soluble Drug. *J. Controlled Release* **1999**, *57*, 171–185.
43. Chan, J. M.; Zhang, L.; Yuet, K. P.; Liao, G.; Rhee, J.-W.; Langer, R.; Farokhzad, O. C. PLGA-Lecithin-PEG Core-Shell Nanoparticles for Controlled Drug Delivery. *Biomaterials* **2009**, *30*, 1627–1634.
44. Danhier, F.; Lecouturier, N.; Vroman, B.; Jérôme, C.; Marchand-Brynaert, J.; Feron, O.; Préat, V. Paclitaxel-Loaded PEGylated PLGA-Based Nanoparticles: *In Vitro* and *in Vivo* Evaluation. *J. Controlled Release* **2009**, *133*, 11–17.
45. D'Addio, S. M.; Prud'homme, R. K. Controlling Drug Nanoparticle Formation by Rapid Precipitation. *Adv. Drug Delivery Rev.* **2011**, *63*, 417–426.
46. Ganachaud, F.; Katz, J. L. Nanoparticles and Nanocapsules Created Using the Ouzo Effect: Spontaneous Emulsification as an Alternative to Ultrasonic and High-Shear Devices. *ChemPhysChem* **2005**, *6*, 209–216.
47. Hornig, S.; Heinze, T.; Becer, C. R.; Schubert, U. S. Synthetic Polymeric Nanoparticles by Nanoprecipitation. *J. Mater. Chem.* **2009**, *19*, 3838–3840.
48. Aubry, J.; Ganachaud, F.; Cohen Addad, J.-P.; Cabane, B. Nanoprecipitation of Polymethylmethacrylate by Solvent Shifting: 1. Boundaries. *Langmuir* **2009**, *25*, 1970–1979.
49. Perevyazko, I. Y.; Vollrath, A.; Pietsch, C.; Schubert, S.; Pavlov, G. M.; Schubert, U. S. Nanoprecipitation of Poly(methyl Methacrylate)-Based Nanoparticles: Effect of the Molar Mass and Polymer Behavior. *J. Polym. Sci., Part A: Polym. Chem.* **2012**, *50*, 2906–2913.
50. De Oliveira, A. M.; Jäger, E.; Jäger, A.; Stepánek, P.; Giacomelli, F. C. Physicochemical Aspects behind the Size of Biodegradable Polymeric Nanoparticles: A Step Forward. *Colloids Surf., A* **2013**, *436*, 1092–1102.
51. Perevyazko, I.; Vollrath, A.; Hornig, S.; Pavlov, G. M.; Schubert, U. S. Characterization of Poly(methyl Methacrylate) Nanoparticles Prepared by Nanoprecipitation Using Analytical Ultracentrifugation, Dynamic Light Scattering, and Scanning Electron Microscopy. *J. Polym. Sci., Part A: Polym. Chem.* **2010**, *48*, 3924–3931.
52. Schneider, J.; Jallouk, A. P.; Vasquez, D.; Thomann, R.; Forget, A.; Pino, C. J.; Shastri, V. P. Surface Functionality as a Means to Impact Polymer Nanoparticle Size and Structure. *Langmuir* **2013**, *29*, 4092–4095.
53. Seremeta, K. P.; Chiappetta, D. A.; Sosnik, A. Poly(epsilon-Caprolactone), Eudragit (R) RS 100 and Poly(epsilon-caprolactone)/Eudragit (R) RS 100 Blend Submicron Particles for the Sustained Release of the Antiretroviral Efavirenz. *Colloids Surf., B* **2013**, *102*, 441–449.
54. Koynov, K.; Butt, H.-J. Fluorescence Correlation Spectroscopy in Colloid and Interface Science. *Curr. Opin. Colloid Interface Sci.* **2012**, *17*, 377–387.
55. Klymchenko, A. S.; Roger, E.; Anton, N.; Anton, H.; Shulov, I.; Vermot, J.; Mely, Y.; Vandamme, T. F. Highly Lipophilic Fluorescent Dyes in Nano-Emulsions: Towards Bright Non-Leaking Nano-Droplets. *RSC Adv.* **2012**, *2*, 11876–11886.
56. Hühn, D.; Kantner, K.; Geidel, C.; Brandholt, S.; De Cock, I.; Soenen, S. J. H.; Rivera_Gil, P.; Montenegro, J.-M.; Braeckmans, K.; Müllen, K.; *et al.* Polymer-Coated Nanoparticles Interacting with Proteins and Cells: Focusing on the Sign of the Net Charge. *ACS Nano* **2013**, *7*, 3253–3263.
57. Ren, W.; Tian, G.; Jian, S.; Gu, Z.; Zhou, L.; Yan, L.; Jin, S.; Yin, W.; Zhao, Y. TWEEN Coated NaYF4:Yb,Er/NaYF4 Core/Shell Upconversion Nanoparticles for Bioimaging and Drug Delivery. *RSC Adv.* **2012**, *2*, 7037–7041.
58. Le Maire, M.; Champeil, P.; Møller, J. V. Interaction of Membrane Proteins and Lipids with Solubilizing Detergents. *Biochim. Biophys. Acta, Biomembr.* **2000**, *1508*, 86–111.

59. Zhang, Y.; Lam, Y. M. Controlled Synthesis and Association Behavior of Graft Pluronic in Aqueous Solutions. *J. Colloid Interface Sci.* **2007**, *306*, 398–404.
60. Vitale, S. A.; Katz, J. L. Liquid Droplet Dispersions Formed by Homogeneous Liquid–Liquid Nucleation: "The Ouzo Effect". *Langmuir* **2003**, *19*, 4105–4110.
61. Lince, F.; Marchisio, D. L.; Barresi, A. A. Strategies to Control the Particle Size Distribution of Poly-E-Caprolactone Nanoparticles for Pharmaceutical Applications. *J. Colloid Interface Sci.* **2008**, *322*, 505–515.
62. Kowalczuk, A.; Trzcinska, R.; Trzebicka, B.; Müller, A. H. E.; Dworak, A.; Tsvetanov, C. B. Loading of Polymer Nanocarriers: Factors, Mechanisms and Applications. *Prog. Polym. Sci.* **2014**, *39*, 43–86.
63. Torchilin, V. P. Micellar Nanocarriers: Pharmaceutical Perspectives. *Pharm. Res.* **2007**, *24*, 1–16.
64. Chorny, M.; Fishbein, I.; Danenberg, H. D.; Golomb, G. Lipophilic Drug Loaded Nanospheres Prepared by Nanoprecipitation: Effect of Formulation Variables on Size, Drug Recovery and Release Kinetics. *J. Controlled Release* **2002**, *83*, 389–400.
65. Contado, C.; Vighi, E.; Dalpiaz, A.; Leo, E. Influence of Secondary Preparative Parameters and Aging Effects on PLGA Particle Size Distribution: A Sedimentation Field Flow Fractionation Investigation. *Anal. Bioanal. Chem.* **2013**, *405*, 703–711.
66. Khoee, S.; Yaghoobian, M. An Investigation into the Role of Surfactants in Controlling Particle Size of Polymeric Nanocapsules Containing Penicillin-G in Double Emulsion. *Eur. J. Med. Chem.* **2009**, *44*, 2392–2399.
67. Redhead, H. M.; Davis, S. S.; Illum, L. Drug Delivery in Poly(lactide-Co-Glycolide) Nanoparticles Surface Modified with Poloxamer 407 and Poloxamine 908: *In Vitro* Characterisation and *in Vivo* Evaluation. *J. Controlled Release* **2001**, *70*, 353–363.
68. Duy, J.; Connell, L. B.; Eck, W.; Collins, S. D.; Smith, R. L. Preparation of Surfactant-Stabilized Gold Nanoparticle–Peptide Nucleic Acid Conjugates. *J. Nanopart. Res.* **2010**, *12*, 2363–2369.
69. Croy, S. R.; Kwon, G. S. Polysorbate 80 and Cremophor EL Micelles Deaggregate and Solubilize Nystatin at the Core–Corona Interface. *J. Pharm. Sci.* **2005**, *94*, 2345–2354.
70. Chaibundit, C.; Ricardo, N. M. P. S.; Costa, F.; de, M. L. L.; Yeates, S. G.; Booth, C. Micellization and Gelation of Mixed Copolymers P123 and F127 in Aqueous Solution. *Langmuir* **2007**, *23*, 9229–9236.
71. Schubert, S.; Delaney, J. T.; Schubert, U. S. Nanoprecipitation and Nanoformulation of Polymers: From History to Powerful Possibilities beyond Poly(lactic Acid). *Soft Matter* **2011**, *7*, 1581–1588.
72. Nehilla, B. J.; Allen, P. G.; Desai, T. A. Surfactant-Free, Drug-Quantum-Dot Coloaded Poly(lactide-Co-Glycolide) Nanoparticles: Towards Multifunctional Nanoparticles. *ACS Nano* **2008**, *2*, 538–544.
73. Trofymchuk, K.; Reisch, A.; Shulov, I.; Mély, Y.; Klymchenko, A. S. Tuning the Color and Photostability of Perylene Diimides Inside Polymer Nanoparticles: Towards Biodegradable Substitutes of Quantum Dots. *Nanoscale* **2014**, *6*, 12934–12942.
74. Clamme, J. P.; Azoulay, J.; Mély, Y. Monitoring of the Formation and Dissociation of Polyethylenimine/DNA Complexes by Two Photon Fluorescence Correlation Spectroscopy. *Biophys. J.* **2003**, *84*, 1960–1968.